AAC Accepts, published online ahead of print on 4 August 2014
Antimicrob. Agents Chemother. doi:10.1128/AAC.02765-14

Title:

Nitro/nitrosyl ruthenium complexes are potent and selective anti-*Trypanosoma cruzi* agents causing autophagy and necrotic parasite death

Running title:

Trypanocidal ruthenium complexes

Authors:

Tanira M. Bastos[a], Marília I. F. Barbosa[b], Monize M. da Silva[b], José W. da C. Júnior,[b] Cássio S. Meira[a], Elisalva T. Guimaraes[a,c], Javier Ellena[d], Diogo R. M. Moreira[a,e], Alzir A. Batista[b], Milena B. P. Soares[a,e*]

[a]FIOCRUZ, Centro de Pesquisas Gonçalo Moniz, CEP 40296-710, Salvador, BA, Brazil. [b]UFSCAR, Departamento de Química, 13565-905, São Carlos, SP, Brazil. [c]UNEB, Departamento de Ciências da Vida, 41150-000, Salvador, BA, Brazil. [d]USP, Instituto de Física de São Carlos, CEP 13560-970, São Carlos, SP, Brazil. [e]Centro de Biotecnologia e Terapia Celular, Hospital São Rafael, 41253-190, Salvador, BA, Brazil.

*Corresponding authors: FIOCRUZ, Centro de Pesquisas Gonçalo Moniz, CEP 40296-710, Salvador, BA, Brazil. (+55)31762292; email: milenabpsoares@gmail.com

ABSTRACT

The *cis*–[RuCl(NO_2)(dppb)(5,5'–mebipy)] (**1**), *cis*–[Ru(NO_2)$_2$(dppb)(5,5'–mebipy)] (**2**), *ct*–[RuCl(NO)(dppb)(5,5'–mebipy)](PF_6)$_2$ (**3**) and *cc*–[RuCl(NO)(dppb)(5,5'–mebipy)]PF_6 (**4**) complexes, where 5,5'–mebipy = 5,5'–dimethyl–2,2'-bipyridine and dppb = 1,4–*bis*(diphenylphosphino)butane, were synthesized and characterized. The structure of the *cis*–[Ru(NO_2)$_2$(dppb)(5,5'–mebipy)] (**2**) complex was determined by X-ray crystallography. These complexes exhibited a higher anti-*T. cruzi* activity than benznidazole, the current antiparasitic drug. Complex (**3**) was the most potent, displaying EC_{50} = 2.1±0.6 µM against trypomastigotes and IC_{50} = 1.3±0.2 µM against amastigotes, while it displayed a CC_{50} of 51.4±0.2 µM in macrophages. It was observed that the nitrosyl complex (**3**), but not its analog lacking the nitrosyl group, releases nitric oxide into parasite cells. This release has a diminished effect on the trypanosomal protease cruzain, but induces substantial parasite autophagy, which is followed by a series of irreversible morphological impairments to the parasites and finally results in cell death by necrosis. In infected mice, orally administered complex (**3**) (5 x 75 µmol/kg) reduced blood parasitemia and increased the survival rate of the mice. Combination index analysis of complex (**3**) indicated that its in vitro activity against trypomastigotes is synergic with benznidazole. In addition, drug combination enhanced efficacy in infected mice, suggesting that ruthenium- nitrosyl complexes are potential constituents for drug combinations.

Keywords: Chagas disease – *Trypanosoma cruzi* – ruthenium complexes – nitric oxide – autophagy – necrosis.

INTRODUCTION

Chagas disease, caused by the protozoan parasite *Trypanosoma cruzi*, affects approximately 10 million people worldwide, with a high prevalence in Latin America (1). The main drugs used against this disease are benznidazole and nifurtimox (2), both of which are effective in curing the disease when administered during the acute phase, but are less effective in patients that have progressed to the chronic phase (3). Furthermore, these drugs are not considered ideal, due to severe side effects and drug resistance to *T. cruzi* strains have been reported (4). Thus, research aimed at identifying molecules with anti-*T. cruzi* activity is urgently need for the treatment of Chagas disease.

In recent years, a variety of anti-*T. cruzi* drug targets have been identified, including the enzymes lanosterol 14α-demethylase, *trans*-sialidase, trypanothione reductase and cysteine protease (5). *T. cruzi* contains a cysteine protease homologous to cathepsin L in mammalian cells, called cruzipain or cruzain, which is primarily responsible for the proteolytic activity involved in all stages of the parasite's life cycle (6,7). Cruzain is important for parasite survival, cell growth and differentiation (8,9). Furthermore, this enzyme plays an important role in the process of parasite internalization in mammalian cells and in the intracellular replication of *T. cruzi* (7,9).

Nitric oxide (NO) is a well-known endogenous trypanocidal molecule, which contributes to host control of acute infection (10,11). NO inactivates cruzain by *S*-nitrosylation of the binding site (12), but *T. cruzi* uses trypanothione reductase to convert NO into a harmless species (13). Therefore, it has been hypothesized that NO-donor drugs may be useful against *T. cruzi* infection by producing exogenous NO (14). Organic NO-donor molecules have been investigated as anti-*T. cruzi* agents, but compounds with *in vivo* efficacy have not been identified (15). In recent years, ruthenium-nitrosyl complexes have been evaluated as anti-*T. cruzi* agents, demonstrating potent and selective antiparasitic activity including in *T. cruzi*-infected mice (16-19). In addition, this class of complexes exhibited inhibitory activity against the *T. cruzi* glyceraldehyde 3-phosphate

dehydrogenase, suggesting that ruthenium-nitrosyl complexes may have pleiotropic effects (19). From the point of view of medicinal chemistry, ruthenium complexes have been explored as an alternative to platinum complexes in the context of anticancer and anti-infective chemotherapy (20-22). More specifically, ruthenium complexes are described as outstanding bioactive agents because of the phosphine ligands, which provide great stability for these compounds (23-26). Nevertheless, only a few ruthenium complexes containing these ligands have been full examined against *T. cruzi* (19).

Therefore, in this study we evaluated the *in vitro* and *in vivo* anti-*T. cruzi* activity of four new ruthenium complexes: *cis*–[RuCl(NO_2)(dppb)(5,5'–mebipy)] (**1**), *cis*–[Ru(NO_2)$_2$(dppb)(5,5'–mebipy)] (**2**), *ct*–[RuCl(NO)(dppb)(5,5'–mebipy)](PF_6)$_2$ (**3**) and *cc*–[RuCl(NO)(dppb)(5,5'–mebipy)](PF_6)$_2$ (**4**). All the synthesized compounds are mononuclear complexes and contain 5,5'–dimethyl-2,2'–bipyridine (5,5'–mebipy) and 1,4–bis(diphenylphosphino)butane (dppb) ligands. To ascertain the importance of the nitrosyl group in antiparasitic activity, the synthesized complexes contained a nitrosyl group in two different positions (*cis* and *trans*), and two complexes containing a nitro group in the place of nitrosyl. Also, a complex lacking the nitro/nitrosyl groups, denoted *cis*–[$RuCl_2$(dppb)(bipy)] (**5**), was prepared and tested. By testing complexes (**1**–**5**) *in vitro*, a potent anti-*T. cruzi* activity was observed in the nitro/nitrosyl complexes (**1-4**), which was higher than that observed for benznidazole. In contrast, complex (**5**) did not show antiparasitic activity. Complex (**3**), the most potent compound, exhibited strong trypanocidal activity, through the release of NO, which subsequently induced the formation of vacuoles typical of the autophagy process. Moreover, complex (**3**) decreased blood parasitemia in *T. cruzi*-infected mice, strengthening the hypothesis that ruthenium complexes are promising drugs for Chagas disease therapy.

MATERIALS AND METHODS

Synthesis and drug dilution: synthesis, structural characterization and X-ray analysis of complexes (**1-5**) is described in the supporting information section. All complexes as well as the reference drugs were dissolved in

DMSO (Sigma-Aldrich, St. Louis, USA) and then diluted in cell culture medium. The final concentration of DMSO was less than 1 % in all *in vitro* experiments.

Animals: Female BALB/c mice (18–20 g) were maintained in sterilized cages under a controlled environment, receiving a rodent balanced diet and water *ad libitum* at Centro de Pesquisas Gonçalo Moniz (Fundação Oswaldo Cruz, Bahia, Brazil). All experiments were carried out in accordance with the recommendations of Ethical Issues Guidelines and were approved by the local Animal Ethics Committee (protocol number 002/2011).

Parasites: All experiments were performed with the Y strain of *T. cruzi*. The epimastigote form was maintained in axenic media at 28° C, with weekly transfers into liver infusion tryptose (LIT) medium supplemented with 10% fetal bovine serum (FBS; Cultilab, Campinas, Brazil), 1 % hemin (Sigma-Aldrich), 1 % R9 medium (Sigma-Aldrich) and 50 µg/mL of gentamicin (Novafarma, Anápolis, Brazil). For *in vitro* assays, metacyclic trypomastigote form of *T. cruzi* was obtained from the supernatant of infected LLC-MK2 cells and maintained in RPMI-1640 medium (Sigma-Aldrich) supplemented with 10% FBS (Cultilab, Campinas, Brazil) and 50 µg/mL of gentamicin (Novafarma, Anápolis, Brazil) at 37° C with 5 % CO_2. For *in vivo* assays, bloodstream trypomastigotes were obtained from infected BALB/c mice at the peak of parasitemia.

Activity against epimastigotes: The effect of the treatment on epimastigotes proliferation was observed 5 days after incubation with the complexes at six concentrations. Epimastigote forms were resuspended at 5×10^6 cells/mL in supplemented LIT medium. The number of viable parasites were counted in a hemocytometer and complex activity was expressed as IC_{50}, corresponding to the inhibitory concentration at 50 % in comparison to untreated parasites. Each drug concentration was carried out in triplicate and three independent experiments

were performed. The reference drug, benznidazole (Lafepe, Pernambuco, Brazil), was used as the positive control.

Activity against trypomastigotes: Trypomastigotes were cultured in 96-well plates (2×10^6 cells/mL) in enriched RPMI-1640 medium, in the presence or absence of the complexes at different concentrations for 24 h. Viable parasites were counted in a hemocytometer and complex activity was expressed as EC_{50}, corresponding to the effective concentration at 50 % in comparison to untreated parasites. Each drug concentration was carried out in triplicate and three independent experiments were performed. The reference drug, benznidazole, was used as the positive control. For *in vitro* drug combinations**,** doubling dilutions of each drug (ruthenium complex **3** and benznidazole) used alone or in fixed combinations were incubated with 2×10^6 cells/mL trypomastigotes for 24 h. The analysis of the combined effects was performed by calculating the median effect principle using CompuSyn software.

Host cell toxicity: Five days after 3 % sodium thioglycolate injection (Sigma-Aldrich), macrophages were obtained by washing with saline solution in the peritoneal cavity of BALB/c mice. Macrophages in RPMI-1640 medium supplemented with 10 % FBS were seeded on 96-well plate at 5×10^5 cells/mL, treated with the complexes during 6 h or 24 h of incubation time. Following this, cells were washed with PBS twice and cell viability was determined by AlamarBlue assay (Invitrogen, Carlsbad, CA, USA) according to the manufacturer instructions. Colorimetric readings were performed after 10 h at 570 and 600 nm. CC_{50} values were calculated using data-points gathered from three independent experiments.

***In vitro T. cruzi* infection assay:** Peritoneal macrophages stimulated with 3 % sodium thioglycolate (Sigma-Aldrich) were transferred to 24-well plate at 2×10^5 cells/well in supplemented RPMI-1640 medium and maintained overnight at 37 °C with 5 % CO_2. The cultures were washed with saline solution and infected with

trypomastigotes (10:1 parasites to host cells). Following 2 h of incubation, the non-internalized parasites were removed by washing with saline solution and fresh medium, with or without drugs (25, 10, 5 and 1.0 µM), were added to the cultures and incubated for 6 h. Afterwards, the culture was washed with saline and drug-free medium was added and incubated for 4 days. Cells were fixed in absolute ethanol, stained with hematoxylin and eosin and analyzed in an optical microscope (Olympus, Tokyo, Japan). The percentage of infected macrophages and the percentage of intracellular parasites per 100 macrophages were determined and compared to the negative control. The IC_{50} value of proliferation inhibition of amastigotes was calculated using the number of parasites/100 cells. The reference drug, benznidazole, was used as the positive control. Each drug concentration was carried out in triplicate and three independent experiments were performed.

Cruzain inhibition: Recombinant cruzain was activated in acetate buffer (0.1 M; pH 5.5) containing 5.5 mM of DTT (Invitrogen) and the protein concentration was adjusted to a final concentration of 0.1 µM. Protein was incubated in phosphate buffer containing 0.01% Triton 100 and transferred to a 96-well plate. Following complex addition, the plate was incubated for 10 min at 35 °C. A solution containing the protease substrate, Z-FR-AMC (Sigma-Aldrich), was then added and incubated for 10 min, and read using the EnVision multilabel reader (PerkinElmer, CT, USA). The percentage of cruzain inhibition was calculated using the following equation: $100 - (A1/A \times 100)$, where A1 represents the cruzain relative fluorescence unit in the presence of the test inhibitor and A refers to the control RFU (cruzain and substrate only). IC_{50} values of cruzain activity inhibition were also calculated. (2*S*,3*S*)-*trans*-epoxysuccinyl-L-leucylamido-3-methylbutane (E-64c) (Sigma-Aldrich) was used as the reference cruzain inhibitor. Each drug concentration was carried out in triplicate and two independent experiments were performed.

Nitric oxide production: Peritoneal macrophages stimulated with 3 % sodium thioglycolate (10^6 cells/well) were incubated in a 24-well plate and infected with trypomastigotes (10^6 parasites/well) for 2 h. It was also

performed this experiment using J774 macrophages at 10^6 cells/well, which were incubated in a 24-well plate and infected with trypomastigotes (2 x 10^5 parasites/well) for 3 h. Cells were washed with saline solution and treated with complex (**3**) or (**5**) at a concentration of 10 µM for 24 h. For the positive control, cells were stimulated with 5.0 ng/mL of IFN-γ (R&D Systems, Minneapolis, MN, USA) and 500 ng/mL of LPS (Sigma-Aldrich). Nitrite levels were determined 24 h after incubation using the Griess method (27).

Transmission and scanning electron microscopy analysis: Trypomastigotes (10^7 cells/mL) were treated with 2.1 µM of complex (**3**) and incubated for 24 h at 37 °C with 5% CO_2. Infected macrophages were treated with 2.1 µM of complex (**3**) and incubated for 6 h. After incubation, parasites were fixed for 1 h at room temperature with 2% formaldehyde and 2.5% glutaraldehyde (Electron Microscopy Sciences, Hatfield, PA, USA) in sodium cacodylate buffer (0.1 M, pH 7.2). Fixed parasites were then washed 4 times with sodium cacodylate buffer (0.1 M, pH 7.2), and post-fixed with a 1 % solution of osmium tetroxide (Sigma-Aldrich). The cells were dehydrated in an ascending acetone series (30, 50, 70, 90 and 100%) and embedded in PolyBed resin (PolyScience Family, Warrington, PA, USA). Ultrathin sections were prepared on a Leica UC7 ultramicrotome and collected on 300 mesh copper grids, contrasted with uranyl acetate and lead citrate. Images were captured in a JEOL TEM-1230 transmission electron microscope. Alternatively, trypomastigotes were dried by using the critical-point method with CO_2, mounted on aluminum stubs, coated with a 20-nm-thick gold layer, and examined under a JEOL JSM-6390LV scanning electron microscope.

Monodansylcadaverine labeling: Trypomastigotes (10^7 cells/mL) were treated with complex (**3**) at a concentration of 2.1 µM. After incubation for 24 h, 0.05 mM of monodansylcadaverine (MDC, Sigma-Aldrich) was added and incubated for 15 min in the absence of light. For the positive control, cells were treated with 0.1 mg/mL of rapamycin (Sigma-Aldrich). The autophagy inhibitor, wortmannin (Sigma-Aldrich) was used at 0.5

µM and added simultaneously with complex (**3**) to the cell culture. The parasites were washed twice with PBS and analyzed in a FV1000 confocal microscope (Olympus).

LC3B immunolocalization: Infected macrophages (as described above) were treated with complex (**3**) at a concentration of 2.1 µM. Following 6 h of incubation, cells were washed in PBS and fixed with 4 % paraformaldehyde (Electron Microscopy Sciences) for 20 min., permeabilised with 0.2 % Triton X 100 (Sigma-Aldrich) in PBS for 15 min at room temperature and blocked with background blocker (Diagnostic BioSystem, Pleasanton, CA, USA). Cells were incubated overnight with rabbit polyclonal antibody against LC3B (Invitrogen) (1/100 dilution) diluted in PBS/BSA 1 %, rinsed and incubated for 1 h at room temperature with Alexa Fluor® 568-conjugated goat anti-rabbit IgG (Molecular Probes, Carlsbad, CA, USA) diluted to 1:400. Subsequently, cells were washed in PBS and mounting medium with 4',6-diamidino-2-phenylindole - DAPI (Vector Labs, Burlingame, CA, USA). Cells were analyzed by confocal microscopy (FV1000, Olympus).

Flow cytometry analysis: Trypomastigotes (10^7 cells/mL) were resuspended in supplemented RPMI-1640 medium and treated with complex (**3**) (2.1 or 5 µM) for 36 h at 37° C with 5% CO_2. Parasites were labeled with propidium iodide (PI) and annexin V using the annexin V-FITC apoptosis detection kit (Sigma-Aldrich) according to the manufacturer instructions. Experiment was performed using a BD FACS Calibur flow cytometer (San Jose, CA, USA) by acquiring 10,000 events, and data were analyzed by BD CellQuest software (San Jose, CA, USA).

***In vivo* anti-*T. cruzi* activity:** Female BALB/c mice (18-20 g) were infected by intraperitoneal injection of 10^4 bloodstream trypomastigotes of Y strain in 100 µL per mouse. Only mice with positive blood parasitemia were included in the experiment. Each drug was solubilized in DMSO/saline (10:90 v/v) prior administration. Mice were randomly divided into groups, with an n=6. Treatment was initiated within 5 day post-infection and given,

once-a-day orally by gavage for five consecutive days. Complex (**3**) doses were administered at 25 (26.6 mg/kg) or 75 µmol/kg (80 mg/kg), and benznidazole at 384 µmol/kg (100 mg/kg). According to recommendations (28,29), the following parameters were evaluated: (I) microscopic parasitemia analysis at 5, 8, 10 and 12 days post-infection and (II) 30 days post-infection animal survival. The % of parasitemia reduction was calculated as follow ([average vehicle group − average treated group)/average vehicle group] × 100%). Two independent experiments were carried.

***In vivo* drug combinations**: The same in vivo protocol described above was performed. The four groups included were: (I) vehicle DMSO/saline (10:90 v/v), (II) complex (**3**) alone at 75 µmol/kg (80 mg/kg), (III) benznidazole alone at 38 µmol/kg (10 mg/kg) and (IV) simultaneous treatment with complex (**3**) at 75 µmol/kg and benznidazole at 38 µmol/kg. Two independent experiments were carried.

Statistical analyses: Nonlinear regression analysis was used to calculate CC_{50}, EC_{50} and IC_{50} values. The selectivity index (SI) was defined as the ratio of CC_{50} (macrophages) by IC_{50} (amastigote form). One-way ANOVA and Bonferroni multiple comparison tests were used to determine the statistical significance of group comparisons in the *in vitro* infection assay and two-way ANOVA with Bonferroni multiple comparison tests were used in the *in vivo* assay (parasitemia). Results were considered statistically significant when $p < 0.05$. Analyses were performed using GraphPad Prism version 5.01 (Graph Pad Software, San Diego, CA, USA) and OriginPro version 8.5 (OriginLab, Northampton, MA, USA) (cruzain IC_{50} values only). Animal survival rates were analyzed with GraphPad Prism 1.5 (GraphPad Software). Combined drug analysis was calculated by using CompuSyn (ComboSyn, Inc., Paramus, NJ. USA).

RESULTS

Compounds characterization

Panel A of figure 1 shows the structures of ruthenium complexes investigated here. Complex (**1**) is the prototype compound, since it was used as the basis for synthesis of all other compounds. The differences among the complexes are based on the presence or absence of the nitro/nitrosyl group or chlorine. Complex (**1**) has a nitro group and a chlorine ligand; complex (**2**) was formed by replacing the chlorine by a nitro group. Complexes (**3**) and (**4**) are nitrosyl species. The difference between complexes (**3**) and (**4**) is the NO position; in complex (**3**), the NO is *cis* to chlorine and *trans* to phosphorus atoms, whereas in complex (**4**), NO is *cis* to chlorine and *cis* to phosphorus atoms.

All complexes were subjected to chemical and spectroscopic analysis. The elemental composition (C, H and N) of the complexes corresponded closely to the calculated values. The $^{31}P\{^{1}H\}$ NMR spectra of complexes (**1-4**) exhibited a pair of doublets that indicated the magnetic inequivalence of the phosphorus atoms present in the dppb (30). The observed doublets showed chemical shifts different from those of the starting material *cis*-[$RuCl_2$(dppb)(5,5'–mebipy)], suggesting that the presence of the nitro or nitrosyl groups coordinated to the metal shifted the electron density of the phosphorus atoms from the dppb.

In the IR spectrum of *cis*-[RuCl(NO_2)(dppb)(5,5'-mebipy)] (**1**), there were strong bands at 1349 cm^{-1} and 1298 cm^{-1}, which can be assigned to $\nu_{as}NO_2$ and ν_sNO_2, respectively. For the *cis*-[$Ru(NO_2)_2$(dppb)(5,5'–mebipy)] (**2**), these bands were at 1360 cm^{-1} and 1310 cm^{-1} ($\nu_{as}NO_2$), and at 1294 cm^{-1} and 1269 cm^{-1} (ν_sNO_2). The presence of four bands for this complex indicates that nitro groups are non-equivalent, being one *trans* to the nitrogen of 5,5`-mebipy, while the other is *trans* to the phosphorus of dppb. The nitrosyl complexes *ct*-[RuCl(NO)(dppb)(5,5-mebipy)]$(PF_6)_2$ (**3**) and *cc*-[RuCl(NO)(dppb)(5,5-mebipy)]$(PF_6)_2$ (**4**) exhibited strong bands at 1891 cm^{-1} and at 1895 cm^{-1}, respectively, which were assigned to the NO^+ stretching (31). Nitro group can be bound to metal through either nitrogen or oxygen, which may produce geometric isomers (32). The *cis*-[RuCl(NO_2)(dppb)(5,5'-mebipy)] (**1**) complex exhibits its ρ_wNO_2 band at 572 cm^{-1}, while *cis*-

[$Ru(NO_2)_2$(dppb)(5,5'–mebipy)] (**2**) has two bands, at 566 and 610 cm^{-1}, suggesting that in both complexes the nitro group is bound to the ruthenium through the nitrogen atom (32,33). In addition to infrared, the electronic absorption spectra for all complexes were characterized by an intense high energy band centered at about 300 nm, which can be assigned to an intra-ligand π–π* transition. Also, these complexes exhibited low-energy bands in the range of 316-488 nm, which can be assigned to a metal-to-ligand charge transfer (MLCT) transition, Ru (dπ) to ligand (π*).

The crystal structure of *cis*-[$Ru(NO_2)_2$(dppb)(5,5'–mebipy)] (**2**) was solved by X-ray crystallography (**Table 1**), and its ORTEP view, was prepared with ORTEP-3 for Windows (**Figure 1**, panel B). Selected bond lengths (Å) and angles (o) in the complex are listed in **Table S1**. The *cis*-[$Ru(NO_2)_2$(dppb)(5,5`-mebipy)] complex exhibits a distorted octahedral geometry, and it crystallized in a triclinic system, space group *P*-1, with the metal center coordinated to two bidentate ligands and two NO_2 groups. The nitro groups are *cis*-positioned relative to each other and coordinated through the nitrogen atoms, as suggested by the IR data. From the data in **Table S1**, it can be seen that the Ru(1)-$N(1)_{(NO2)}$ (Ru-$N_{(NO2)}$ *trans* P) bond length is about 0.5 Å longer than the bond Ru(1)-N(2) [Ru-$N_{(NO2)}$ *trans* $N_{(bipy)}$], which is consistent with the stronger *trans* effect of the phosphorus atoms, relative to the *trans* effect of the nitrogen atoms. Also, this difference explains the two bands for νNO_2 observed in the infrared spectrum of complex (**2**).

Anti-*T. cruzi* activity and host cell cytotoxicity

Anti-*T. cruzi* activity was determined in epimastigotes and trypomastigotes of Y strain and results were expressed as IC_{50} and EC_{50}, respectively. Cell toxicity in BALB/c mice macrophages was performed under identical drug incubation times for antiparasitic assay in trypomastigotes (*i.e.*, 24 h drug exposure) and expressed as CC_{50}. Benznidazole was used as the reference drug in these assays and results are reported in **Table 2**. Benznidazole exhibited an IC_{50} of 10.7±1.6 μM in epimastigote proliferation. Similarly, it was

observed that ruthenium complexes (**2**), (**3**) and (**4**) greatly inhibited epimastigotes. In contrast, complex (**1**) did not inhibit epimastigote proliferation. Complexes (**1**–**4**) decreased trypomastigote viability, with EC_{50} values lower than benznidazole. Complex (**5**), which lacks a nitro/nitrosyl group, did not exhibit antitrypomastigote activity, while complex (**3**) was the most active compound among them, with an EC_{50} of 2.1±0.6 μM. Complexes (**1**) and (**5**) did not demonstrate cytotoxicity in macrophages following the drug exposure, and complex (**2**) displayed relatively low cytotoxicity. Complexes (**3**) and (**4**) had CC_{50} values of 28.5±2.0 and 25.4±0.1 μM respectively.

Evaluation of cruzain inhibition

Due to the previous findings that ruthenium complexes inhibit cruzain, inhibitory activity was measured here for all five complexes in an assay based on competition with *N*α-benzoyl-L-arginine-7-amido-4-methylcoumarin (Z-FR-AMC). (2*S*,3*S*)-*trans*-epoxysuccinyl-L-leucylamido-3-methylbutane (E-64c), which is a high-affinity cruzain inhibitor, was used as reference inhibitor and displayed an IC_{50} of 1.0±0.8 nM. As demonstrated in **Table 2**, complex (**2**) did not inhibit cruzain, while complexes (**1**) and (**5**) presented weak potency, with IC_{50} values as high as 30 μM. Complexes (**3**) and (**4**) showed stronger potency against cruzain, with IC_{50} values of 14.4±6.6 and 0.4±0.1 μM, respectively. Although complex (**4**) was the most potent ruthenium complex, it had lower potency in comparison to E-64c

***In vitro* infection**

After observing that ruthenium complexes inhibit extracellular parasite, we investigated their activity against the intracellular parasite. It was observed that all the nitro/nitrosyl complexes at 10 μM caused a statistically significant reduction in the % of *T. cruzi*-infected macrophages compared to untreated-infected cells (**Figure 2**,

panel A). Complex (**3**) was the most potent of the four compounds tested in reducing the *in vitro* infection. Additionally, all the complexes decreased the mean number of intracellular parasites (**Figure 2**, panel B) as well as the parasite burden (**Figure 2**, panel C). Amastigote IC_{50} was calculated by analyzing the % of infected cells (**Table 3**). Ruthenium complex (**3**) greatly inhibited this percentage, displaying an IC_{50} of 1.3±0.2 µM, while benznidazole displayed an IC_{50} of 14.0±0.3 µM. Cytotoxicity of ruthenium complexes incubated for 6 h in macrophages demonstrated that neither benznidazole nor complex (**1**) are cytotoxic at the tested concentrations (CC_{50} > 100 µM). Complex (**2**) exhibited a low cytotoxicity (CC_{50} = 93.1±7.7 µM) and complexes (**3**) and (**4**) were approximately two-fold more cytotoxic than nitro complex (**2**). The selectivity index (SI) of the ruthenium complexes was calculated and it was observed that, among the complexes tested, complex (**3**) showed the highest SI.

NO level in infected cells

ct–[RuCl(NO)(dppb)(5,5'–mebipy)]$(PF_6)_2$ (**3**) was the most potent and selective antiparasitic ruthenium complex. To investigate whether complex (**3**) is a NO-donor drug, NO levels in infected macrophages were inferred by determining nitrite content. In this assay, infected cells were incubated for 24 h with drugs and the nitrite content was estimated by the Griess method. As shown in **Figure 3** panel A, untreated infected BALB/c macrophages produced low level of NO, whereas stimulus with IFN-γ and LPS induced a significant production of NO. In comparison to untreated-infected cells, treatment with 10 µM complex (**3**) presented a significantly elevation in NO ($p < 0.001$). By contrast, treatment with complex (**5**) did not result in significant production of NO. No measurable NO concentration was observed in a cell-free experiment containing only complex (**3**) plus culture media (data not shown). The same conditions were used in infected J774 cell line and similar results were observed (**Figure 3**, panel B)

Electron microscopy analysis

Trypomastigotes were treated with complex (**3**) and analyzed by scanning electron microscopy (SEM). In comparison with untreated parasites (**Figure 4,** panel A), treatment resulted in parasite shrinkage and caused cell membrane discontinuity and fragmentation (**Figure 4,** panel B). Morphological changes following complex (**3**) treatment were observed in 76 % of the parasite cells. Among these cells, 74 % showed cell shrinkage, 21 % displayed membrane discontinuity and 21 % had membrane fragmentation (data not shown). Next, transmission electron microscopy (TEM) experiments were performed in trypomastigotes, as well as intracellular amastigotes. In comparison with untreated trypomastigotes (**Figure 4**, panel C), parasites in the presence of complex (**3**) exhibited swollen of mitochondria (**Figure 4**, panel D) and loss of the nuclear membrane (**Figure 4**, panel E). In most of the treated trypomastigotes, the presence of atypical cytoplasmic vacuoles, and the formation of myelin-like structures (**Figure 4**, panel F) were observed. The presence of these atypical cytoplasmic vacuoles was also observed in intracellular amastigotes following treatment with the ruthenium complex (**Figure 4,** panel H).

Autophagy markers

The observations by transmission micrographs that ruthenium complex induces the formation of atypical cytoplasmic vacuoles led us to investigate whether the mechanism of action involves autophagy. Trypomastigotes were treated with the complex (**3**) and then incubated with monodansylcadaverine (MDC) to label the autophagic cytosolic vacuoles. In this experiment, untreated parasites were not stained with MDC (**Figure 5**, panel A), while parasites treated with rapamycin, a standard autophagy inducer, were stained (**Figure 5**, panel B). Parasites treated with complex (**3**) were positively stained with MDC (**Figure 5**, panel C). In order to distinguish between autophagic and lysosomal vacuoles, an additional experiment was carried out using the

autophagy inhibitor, wortmannin. MDC-staining during complex (**3**) treatment was blocked in the presence of 0.5 µM wortmannin (data not shown). To the next, the presence of microtubule-associated protein 1b light chain 3 (LC3B) was detected in untreated and treated *T. cruzi*-infected macrophages by incubating with polyclonal antibody anti-LC3B. In this controlled experiment, nuclei were stained with 4′,6-diamidino-2-phenylindole (DAPI) and cells were analyzed by immunofluorescence under a confocal microscope. Untreated infected macrophages did not demonstrate LC3B labeling (**Figure 5**, panel A). In contrast, infected macrophages treated with 0.1 mg/mL rapamycin displayed intracellular parasites labeled for LC3B (**Figure 5**, panel B). Similarly, infected macrophages treated with ruthenium complex (**3**) at 2.1 µM displayed intracellular parasites labeled for LC3B (**Figure 5**, panel C).

Parasite cell death

After observing that ruthenium complexes induce autophagy, we were wondering to know the consequence of autophagy to the parasite cells. To this end, trypomastigotes were incubated with two different concentrations (2.5 and 5.0 µM) of complex (**3**) for 36 h at 37 ^{o}C and then double labeled with annexin V-fluorescein isothiocyanate (FITC) and propidium iodide (PI). Individual cell data were acquired and analyzed by flow cytometry. In comparison to untreated parasites (**Figure 6**, panel A), a concentration-related increase in the percentage of stained parasites was observed after complex (**3**) treatment (**Figure 6**, panels B,C). Parasites treated with complex (**3**) at 5.0 µM showed 34.6 % positively stained cells, of which 26.1 % were necrotic (PI stain alone), 5.6 % were late apoptotic (PI+annexin V) and 2.9 % early apoptotic (annexin staining alone). As shown in **Figure 6** panel D, this ruthenium complex significantly increased the proportion of necrotic *T. cruzi* cells in a concentration-dependent manner.

***In vivo* efficacy study**

Complex (**3**) was tested in *T. cruzi*-infected mice during the acute phase. Control groups, receiving either benznidazole or vehicle were included in this experiment. In this assay, 10^4 Y strain trypomastigotes in 100 µL were intraperitoneally inoculated in female BALB/c mice (*n*=6/group). Treatments were given orally by gavage. Blood parasitemia and survival rates were analyzed. In comparison to untreated group, complex (**3**) at 25 and 75 µmol/kg was able to decrease the blood parasitemia peak by 25 % (p <0.001) and 46 % (p <0.001), respectively (**Figure 7**, panel A). On day 12 post-infection, no parasites were detected by microscopic examination in benznidazole group blood samples, indicating negative parasitemia. But the same was not observed for infected mice receiving 75 µmol/kg of complex (**3**). Mice mortality rates were monitored up to 30 days post-infection. When compared to the untreated group, complex (**3**) at 75 µmol/kg significantly decreased mortality (log rank, p < 0.01). The group treated with benznidazole had 100 % survival, while the group treated with the highest dose of complex (**3**) showed a survival rate of 50 % (**Figure 7**, panel B).

Drug combination

Considering that complex (3) and benznidazole exhibit different mechanism of antiparasitic actions, the possibility of drug combination was studied. Complex (**3**) and benznidazole alone or in fixed combinations were evaluated against trypomastigote cell cultures, results were analyzed by CompuSyn software and listed in **Table 4**. In comparison to individual drug incubation, the combination of complex (**3**) and benznidazole reduced both EC_{50} and EC_{90} values. Combination index (CI) calculations was used as cutoff and revealed that this combination has synergistic effects against trypomastigotes. It was observed that drug combinations at the EC_{50} values reduced the % of viable trypomastigotes (**Figure 7,** panel C) but did not reduce the % of viable macrophages (**Figure 7,** panel D). Of note, macrophage cytotoxicity was observed when drug combinations were evaluated in concentrations equal or higher than the EC_{90} values.

Based on the *in vitro* synergism, we evaluated the efficacy of ruthenium complex (**3**) in combination with a sub-optimal dose of benznidazole. Complex (**3**) at 75 µmol/kg (80 mg/kg) and benznidazole at 38 µmol/kg (10 mg/kg) were administrated individually or in combination using the *in vivo* protocol described above. In comparison to the untreated group, benznidazole at this sub-optimal dose reduced blood parasitemia, however did not eliminate circulating parasites. The drug-combination-receiving group presented lower parasitemia than untreated group and groups receiving each individual drug (**Figure 7**, panel E). When monitored for up to 30 days post-infection, the group treated with drug combination had 100 % survival, while the groups treated with each drug alone showed a survival rate of 60 % (**Figure 7**, panel F).

DISCUSSION

Identification of new pharmaceutical is vital for Chagas disease treatment. In order to reach this objective, investigations cannot be limited to small organic molecules, but should also include metallic compounds. In fact, coordination complexes and organometallics are recognized as notable anti-*T. cruzi* agents. For instance, the coordination of trypanocidal molecules with metals increases anti-*T. cruzi* activity in comparison with the metal-free molecules. This enhanced activity can be explained by the gain in lipophilicity. This strategy has been performed to enhance the potency of ketoconazole, clotrimazole, benznidazole, risedronate and quinolones (34-39). Alternatively, metal complexes which are composed of ligands with unique chemical properties (redox and electrochemical behavior based on ligand reductions) exhibit anti-*T. cruzi* properties, possibly due to parasite membrane accumulation, in addition to effects on DNA and enzymes (40-43).

Here the *in vitro* screening of anti-*T. cruzi* activity demonstrated that both nitro and nitrosyl ruthenium complexes are toxic for trypomastigotes and inhibited epimastigote proliferation at non-cytotoxic concentrations in host cells. In contrast, the ruthenium complex lacking nitro and nitrosyl groups did not display anti-*T. cruzi*

activity. Regarding structure-activity relationships, the complex containing two nitro groups was more potent than the complex containing only one. However, the nitrosyl complexes showed greater activity than nitro complexes. This suggests that a nitrosyl group contributes more to antiparasitic activity than a nitro group. For cruzain, nitro complexes exhibited weak or no inhibitory activity, while nitrosyl complexes exhibited greater inhibitory activity. The nitrosyl complex (**4**) was only twice less potent antiparasitic than its isomer (**3**), but it presented much higher potency against cruzain than (**3**). These observations indicate that the environment surrounding the metal is important for biological activity.

After determining that these ruthenium complexes inhibit extracellular *T. cruzi*, we examined their activity in infected macrophages. The complexes were able to reduce the number of infected cells more efficiently than benznidazole, and they clearly arrested parasite growth and differentiation inside the host cells. Given the potency of complex (**3**) against amastigotes, we investigated its mechanism of action in parasites. We observed that nitrosyl complex (**3**) increased the NO levels in infected macrophages, while the complex lacking the nitrosyl group did not. The antiparasitic activity of ruthenium complex (**3**) is likely due to its NO-releasing ability or alternatively by indirectly inducing the NO production. According to the literature, NO release leads to the inactivation of the protease cruzain in parasite cells. However, complex (**3**) did not present potency as strong as the powerful cruzain inhibitor, E-64c. Therefore, we believe that while complex (**3**) is a NO-donor drug, this property is not related to its ability to inhibit cruzain. Further evidence regarding the mechanism of action of complex (**3**) was found by analyzing the parasite ultrastructure and morphology. Two main effects were observed in the treated parasites: first, cell membrane discontinuity and fragmentation, and to a less content, nuclear membrane alterations; second, the appearance of atypical cytoplasmic vacuoles, as well as the formation of myelin-like figures.

Lack of cell membrane integrity is very often associated with necrotic parasite death (44). In fact, parasites treated with complex (**3**) exhibited a cell death pattern via necrosis, rather than apoptosis. Our results are consistent with previous findings demonstrating that ruthenium bipyridyl complexes are prone to

accumulate in the cell membrane (22). The presence of cytoplasmic vacuoles and myelin-like figures suggested that ruthenium complexes induce parasite autophagy. By assaying MDC-staining and LC3B immunolocalization (45,46), it was observed that trypomastigotes were stained with MDC after ruthenium complex treatment and this process was blocked by the presence of the autophagy inhibitor, wortmannin. Similar to the literature (47,48), here ruthenium complex treatment resulted in the accumulation of LC3B in intracellular amastigotes. The findings observed here support the overall idea that nitrosyl-ruthenium complexes release NO, which triggers cellular events, including parasite autophagy. As a result, a number of irreversible morphological impairments occur to the parasite cells, finally leading to cell death by necrosis.

Due to the strong antiparasitic activity of complex (**3**), it was evaluated in mice during the acute phase of Chagas disease. Complex (**3**) had a dose-dependent effect and presented an optimal efficacy when regime was given orally at 75 µmol/kg. This reduced the blood parasitemia and increased mice survival, however, it did not eliminate parasites present in the bloodstream, while the benznidazole regime did. Given the substantial dedication that have been made to identify optimal drug combinations for the treatment of Chagas disease (49,50), a combination of ruthenium complex (**3**) and benznidazole would offer a potential therapy to reduce the benznidazole dosage required to cure infection. This is supported by the fact that combination would target *T. cruzi* at two different modes of action: NO release and autophagy induction mediated by complex (**3**) and nitroreductase inhibition and oxidative stress induction mediated by benznidazole (51,52). *In vitro*, combinations of complex (**3**) and benznidazole were synergic in killing trypomastigotes. In infected mice, combination of ruthenium complex with a sub-optimal dose of benznidazole exhibited enhanced efficacy in terms of reducing infection and increasing survival when compared to each drug used alone. Overall, these findings indicate that ruthenium complexes are a class of suitable constituents for drug combination.

CONCLUSIONS

We investigated the NO-donor drug strategy by synthesizing new ruthenium complexes that feature nitro or nitrosyl groups. These complexes exhibited a broad spectrum of activities (vector-borne stage, bloodstream form, intracellular stage) against *T. cruzi*. This activity is abolished once nitro and nitrosyl groups are removed from the complex, indicating these groups are structural determinants for activity. By examining the underlying mechanism of action of these complexes, it was observed that they release NO, causing autophagy, which is followed by a series of irreversible morphological impairments to the parasites, culminating in necrotic cell death. More striking, ruthenium-nitrosyl complex (**3**) was efficient in reducing blood parasitemia in acutely infected mice and presented synergic effect when in combination with benznidazole.

ACKNOWLEDGEMENTS

This research was funded by CNPq, FAPESB and FAPESP. A.A.B., J.E. and M.B.P.S. are recipients of a CNPq fellowship. T.M.B received a CAPES scholarship; C.S.M. and D.R.M.M. are receiving FAPESB scholarships. We are thankful to Dr. Carine Azevedo for assistance with confocal microscope, Dr. Adriano Alcantara for providing cruzain and Dr. Marcos Vannier dos Santos for providing MDC and rapamycin. We are thankful to the electron microscopy unit of CPqGM.

TRANSPARENCY DECLARATIONS

The authors declare no competing financial interest.

CONTRIBUTING AUTHORS

TMB designed and performed most experimental studies and analyses; MIFB, JWCJ and MMS synthesized and validated the complexes; JE assisted with X-ray crystallography; CSM assisted with the Transmission Electron Microscopy analyses and cell culture; ETG assisted with flow cytometry; DRMM provided guidance and assisted with experimental design and assisted with manuscript preparation, AAB and MBPS initiated the project and provided guidance for experimental design, interpretation of data and preparation of the manuscript. All authors have read and approved the final manuscript.

REFERENCES

1. **Schofield CJ, Jannin J, Salvatella R.** 2006. The future of Chagas disease control. Trends Parasitol. **12**:583–588. Doi: 10.1016/j.pt.2006.09.011
2. **Rodrigues Coura J.** 2013. Chagas disease: control, elimination and eradication. Is it possible? Mem. Inst. Oswaldo Cruz. **108**:962–967. Doi: 10.1590/0074-0276130565
3. **Pinazo MJ, Muñoz J, Posada E, López-Chejade P, Gállego M, Ayala E, del Cacho E, Soy D, Gascon J.** 2010. Tolerance of benznidazole in treatment of Chagas` disease in adults. Antimicrob. Agents Chemother. **54**: 4896−4899. Doi: 10.1128/AAC.00537-10
4. **Urbina JA.** 2010. Specific chemotherapy of Chagas disease: relevance, current limitations and new approaches. Acta Trop. **115**: 55–68. Doi: 10.1016/j.actatropica.2009.10.023
5. **Moreira DRM, Leite ACL, dos Santos RR, Soares MBP.** 2009. Approaches for the development of new anti-*Trypanosoma cruzi* agents. Curr. Drug Targets **10**: 212−231. Doi: 10.2174/138945009787581140
6. **Scharfstein J, Schechter M, Senna M, Peralta JM, Mendonça-Previato L, Miles MA.** 1986. *Trypanosoma cruzi*: characterization and isolation of a 57/51,000 m.w. surface glycoprotein (GP57/51) expressed by epimastigotes and bloodstream trypomastigotes. J. Immunol. **137**: 1336–1341.

7. **Souto-Padrón T, Campetella OE, Cazzulo JJ, de Souza W.** 1990. Cysteine proteinase in *Trypanosoma cruzi*: immunocytochemical localization and involvement in parasite-host cell interaction. J. Cell Sci. **96**: 485–490. Doi: not available.

8. **McKerrow JH, Caffrey C, Kelly B, Loke P, Sajid M.** 2006. Proteases in parasitic diseases. Annu. Rev. Pathol. **1**: 497–536. Doi: 10.1146/annurev.pathol.1.110304.100151

9. **Doyle PS, Zhou YM, Hsieh I, Greenbaum DC, McKerrow JH, Engel JC.** 2011. The *Trypanosoma cruzi* protease cruzain mediates immune evasion. Plos Pathog. **7**: e1002139. Doi: 10.1371/journal.ppat.1002139

10. **Gazzinelli RT, Oswald IP, Hieny S, James SL, Sher A.** 1992. The microbicidal activity of interferon-gamma-treated macrophages against *Trypanosoma cruzi* involves an L-arginine-dependent, nitrogen oxide-mediated mechanism inhibitable by interleukin-10 and transforming growth factor-beta. Eur. J. Immunol. **22**: 2501–2506. Doi: 10.1002/eji.1830221006

11. **Vespa GN, Cunha FQ, Silva, JS.** 1994. Nitric oxide is involved in control of *Trypanosoma cruzi*-induced parasitemia and directly kills the parasite in vitro. Infect. Immun. **62**: 5177–5182. Doi: not available.

12. **Venturini G, Salvati L, Muolo M, Colasanti M, Gradoni L, Ascenzi P.** 2000. Nitric oxide inhibits cruzipain, the major papain-like cysteine proteinase from *Trypanosoma cruzi*. Biochem. Biophys. Res. Commun. **270**: 437–441. Doi: 10.1006/bbrc.2000.2447

13. **Bocedi A, Dawood KF, Fabrini R, Federici G, Gradoni L, Pedersen JZ, Ricci G.** 2010. Trypanothione efficiently intercepts nitric oxide as a harmless iron complex in trypanosomatid parasites. FASEB J. **24**: 1035–1042. Doi: 10.1096/fj.09-146407

14. **Tfouni E, Truzzi DR, Tavares A, Gomes AJ, Figueiredo LE, Franco DW.** 2012. Biological activity of ruthenium nitrosyl complexes. Nitric Oxide **26**: 38–53. Doi: 10.1016/j.niox.2011.11.005

15. **Ascenzi P, Bocedi A, Gentile M, Visca P, Gradoni L.** 2004. Inactivation of parasite cysteine proteinases by the NO-donor 4-(phenylsulfonyl)-3-((2-(dimethylamino)ethyl)thio)-furoxan oxalate. Biochim. Biophys. Acta. **1703**: 69–77. Doi: 10.1016/j.bbapap.2004.09.027

16. **Silva JJ, Osakabe AL, Pavanelli WR, Silva JS, Franco DW.** 2007. In vitro and in vivo antiproliferative and trypanocidal activities of ruthenium NO donors. Br. J. Pharmacol. **152**: 112–121. Doi: 10.1038/sj.bjp.0707363

17. **Silva JJ, Pavanelli WR, Pereira JC, Silva JS, Franco DW.** 2009. Experimental chemotherapy against *Trypanosoma cruzi* infection using ruthenium nitric oxide donors. Antimicrob. Agents Chemother. **53**: 4414–4421. Doi: 10.1128/AAC.00104-09

18. **Guedes PM, Oliveira FS, Gutierrez FR, da Silva GK, Rodrigues GJ, Bendhack LM, Franco DW, Do Valle Matta MA, Zamboni DS, da Silva RS, Silva JS.** 2010. Nitric oxide donor *trans*-[RuCl([15]aneN)NO] as a possible therapeutic approach for Chagas' disease. Br. J. Pharmacol. **160**: 270–282. Doi: 10.1111/j.1476-5381.2009.00576.x

19. **Silva JJ, Guedes PM, Zottis A, Balliano TL, Nascimento Silva FO, França Lopes LG, Ellena J, Oliva G, Andricopulo AD, Franco DW, Silva JS.** 2010. Novel ruthenium complexes as potential drugs for Chagas's disease: enzyme inhibition and in vitro/in vivo trypanocidal activity. Br. J. Pharmacol. **160**: 260–269. Doi: 10.1111/j.1476-5381.2009.00524.x

20. **Levina A, Mitra A, Lay PA.** 2009. Recent developments in ruthenium anticancer drugs. Metallomics **1**: 458-470. Doi: 10.1039/b904071d

21. **Bergano A, Sava G.** 2011. Ruthenium anticancer compounds: myths and realities of the emerging metal-based drugs. Dalton Trans. **40**: 7817-7823. Doi: 10.1039/c0dt01816c

22. **Zava O, Zakeeruddin SM, Danelon C, Vogel H, Grätzel M, Dyson PJ.** 2009. A cytotoxic ruthenium tris(bipyridyl) complex that accumulates at plasma membranes. ChemBioChem **10**: 1796–1800. Doi: 10.1002/cbic.200900013

23. **Groessl M, Zava O, Dyson PJ.** 2011. Cellular uptake and subcellular distribution of ruthenium-based metallodrugs under clinical investigation versus cisplatin. Metallomics **3**: 591–599. Doi: 10.1039/c0mt00101e

24. **Heinrich TA, Von Poelhsitz G, Reis RI, Castellano EE, Neves A, Lanznaster M, Machado SP, Batista AA, Costa-Neto CM.** 2011. A new nitrosyl ruthenium complex: synthesis, chemical characterization, in vitro and in vivo antitumor activities and probable mechanism of action. Eur. J. Med. Chem. **46**: 3616–3622. Doi: 10.1016/j.ejmech.2011.04.064

25. **Pavan FR, Poelhsitz GV, Barbosa MI, Leite SR, Batista AA, Ellena J, Sato LS, Franzblau SG, Moreno V, Gambino D, Leite CQ.** 2011. Ruthenium(II) phosphine/diimine/picolinate complexes: inorganic compounds as agents against tuberculosis. Eur. J. Med. Chem. **46**: 5099–50107. Doi: 10.1016/j.ejmech.2011.08.023

26. **Santos ER, Mondelli MA, Pozzi LV, Corrêa RS, Salistre-de-Araújo SS, Pavan FR, Leite CQF, Ellena J, Malta VRS, Machado SP, Batista AA.** 2013. New ruthenium(II)/phosphines/diimines complexes: promising antitumor (human breast cancer) and *Mycobacterium tuberculosis* fighting agents. Polyhedron **51**: 292–297. Doi: 10.1016/j.poly.2013.01.004

27. **Green LC, Wagner DA, Glogowski J, Skipper PL, Wishnok JS, Tannenbaum SR.** Analysis of nitrate, nitrite, and [^{15}N]nitrate in biological fluids. Anal. Biochem. **126**:131–138.

28. **Brener, Z.** 1962. Therapeutic activity and criterion of cure on mice experimentally infected with *Trypanosoma cruzi*. Rev. Inst. Med. Trop. Sao Paulo. **4**:386–396. Doi: not available.

29. **Romanha, A J, Castro, SL, Soeiro, MN, Lannes-Vieira J, Ribeiro I, Talvani A, Bourdin B, Blum B, Olivieri B, Zani C, Spadafora C, Chiari E, Chatelain E, Chaves G, Calzada JE, Bustamante JM, Freitas-Junior LH, Romero LI, Bahia MT, Lotrowska M, Soares MBP, Andrade SG, Armstrong T, Degrave W, Andrade ZA.** 2010. In vitro and in vivo experimental models for drug

screening and development for Chagas disease. Mem. Inst. Oswaldo Cruz. **105**:233−238. Doi: 10.1590/S0074-02762010000200022

30. **Barbosa MIF, Corrêa RS, Oliveira KM, Rodrigues C, Ellena J, Nascimento OR, Rocha VPC, Nonato FR, Macedo TS, Barbosa-Filho JM, Soares MBP, Batista AA.** 2014. Antiparasitic activities of novel ruthenium/lapachol complexes. J. Inorg. Biochem. **136**: 33–39. Doi: 10.1016/j.jinorgbio.2014.03.009
31. **Richter-Addo G B, Legzdins P.** 1992. Metal nitrosyls. 383 p. Oxford University Press, New York.
32. **Godwin JB, Meyer TJ.** 1971. Nitrosyl-nitrite, interconversion in ruthenium complexes. Inorg. Chem. **10**:2150-2153. Doi: 10.1021/ic50104a012
33. **Nakamoto K.** 1997. Infrared and Raman spectra of inorganic and coordination compounds. 384 p. 5th ed. Part B. Wiley-Interscience, New York.
34. **Navarro M, Cisneros-Fajardo EJ, Lehmann T, Sánchez-Delgado RA, Atencio R, Silva P, Lira R, Urbina JA.** 2001. Toward a novel metal-based chemotherapy against tropical diseases. 6. Synthesis and characterization of new copper(II) and gold(I) clotrimazole and ketoconazole complexes and evaluation of their activity against *Trypanosoma cruzi*. Inorg. Chem. **40**:6879–6884. Doi: 10.1021/ic0103087
35. **Nogueira Silva JJ, Pavanelli WR, Gutierrez FR, Alves Lima FC, Ferreira da Silva AB, Santana Silva J, Wagner Franco D.** 2007. Complexation of the anti-*Trypanosoma cruzi* drug benznidazole improves solubility and efficacy. J. Med, Chem. **51**:4104–4114. Doi: 10.1021/jm701306r
36. **Demoro B, Caruso F, Rossi M, Benítez D, Gonzalez M, Cerecetto H, Parajón-Costa B, Castiglioni J, Galizzi M, Docampo R, Otero L, Gambino D.** 2010. Risedronate metal complexes potentially active against Chagas disease. J. Inorg. Biochem. **104**:1252–1258. Doi: 10.1016/j.jinorgbio.2010.08.004
37. **Reis DC, Pinto MC, Souza-Fagundes EM, Rocha LF, Pereira VR, Melo CM, Beraldo H.** 2011. Investigation on the pharmacological profile of antimony(III) complexes with hydroxyquinoline

derivatives: anti-trypanosomal activity and cytotoxicity against human leukemia cell lines. Biometals **24**: 595–601. Doi: 10.1007/s10534-011-9407-8

38. **Martínez A, Carreon T, Iniguez E, Anzellotti A, Sánchez A, Tyan M, Sattler A, Herrera L, Maldonado RA, Sánchez-Delgado RA.** 2012. Searching for new chemotherapies for tropical diseases: ruthenium-clotrimazole complexes display high in vitro activity against *Leishmania major* and *Trypanosoma cruzi* and low toxicity toward normal mammalian cells. J. Med. Chem. **55**: 3867–3877. Doi: 10.1021/jm300070h
39. **Iniguez E, Sánchez A, Vasquez MA, Martínez A, Olivas J, Sattler A, Sánchez-Delgado RA, Maldonado RA**. 2013. Metal-drug synergy: new ruthenium(II) complexes of ketoconazole are highly active against *Leishmania major* and *Trypanosoma cruzi* and nontoxic to human or murine normal cells. J. Biol. Inorg. Chem. **18**:779-90. Doi: 10.1007/s00775-013-1024-2
40. **Lowe G, Droz AS, Vilaivan T, Weaver GW, Tweedale L, Pratt JM, Rock P, Yardley V, Croft SL.** 1999. Cytotoxicity of (2,2':6',2"-terpyridine)platinum(II) complexes to *Leishmania donovani*, *Trypanosoma cruzi*, and *Trypanosoma brucei*. J. Med. Chem. **42**: 999–1006. Doi: 10.1021/jm981074c
41. **Vieites M, Smircich P, Parajón-Costa B, Rodríguez J, Galaz V, Olea-Azar C, Otero L, Aguirre G, Cerecetto H, González M, Gómez-Barrio A, Garat B, Gambino D.** 2008. Potent in vitro anti-*Trypanosoma cruzi* activity of pyridine-2-thiol *N*-oxide metal complexes having an inhibitory effect on parasite-specific fumarate reductase. J. Biol. Inorg. Chem. **13**: 723–735. Doi: 10.1007/s00775-008-0358-7
42. **Donnici CL, Araujo MH, Oliveira HS, Moreira, DRM, Pereira VRA, Souza MA, De-Castro MCAB, Leite ACL.** 2009. Ruthenium complexes endowed with potent anti-*Trypanosoma cruzi* activity: Synthesis, biological characterization and structure–activity relationships. Bioorg. Med. Chem. **17**:5038-5043. Doi: 10.1016/j.bmc.2009.05.071

43. **Benítez J, Becco L, Correia I, Leal SM, Guiset H, Pessoa JC, Lorenzo J, Tanco S, Escobar P, Moreno V, Garat B, Gambino D.** 2011. Vanadium polypyridyl compounds as potential antiparasitic and antitumoral agents: new achievements. J. Inorg. Biochem. **105**: 303–312. Doi: 10.1016/j.jinorgbio.2010.11.001
44. **Vannier-Santos MA, de Castro SL.** 2009. Electron microscopy in antiparasitic chemotherapy: a (close) view to a kill. Curr. Drug Targets **10**: 246–260. Doi: 10.2174/138945009787581168
45. **Jimenez V, Paredes R, Sosa MA, Galanti N.** 2008. Natural programmed cell death in *T. cruzi* epimastigotes maintained in axenic cultures. J. Cell. Biochem. **105**: 688–98. Doi: 10.1002/jcb.21864
46. **Veiga-Santos P, Barrias ES, Santos JF, de Barros-Moreira TL, de Carvalho TM, Urbina JA, de Souza W.** 2012. Effects of amiodarone and posaconazole on the growth and ultrastructure of *Trypanosoma cruzi*. Int. J. Antimicrob. Agents. **40**: 61–71. Doi: 10.1016/j.ijantimicag.2012.03.009
47. **Tan C, Lai S, Wu S, Hu S, Zhou L, Chen Y, Wang M, Zhu Y, Lian W, Peng W, Ji L, Xu A.** 2010. Nuclear permeable ruthenium(II) β-carboline complexes induce autophagy to antagonize mitochondrial-mediated apoptosis. J. Med. Chem. **53**: 7613–7624. Doi: 10.1021/jm1009296
48. **Castonguay A, Doucet C, Juhas M, Maysinger D.** 2012. New ruthenium(II)-letrozole complexes as anticancer therapeutics. J. Med. Chem. **55**: 8799–8806. Doi: 10.1021/jm301103y
49. **Cencig S, Coltel N, Truyens C, Carlier Y**. 2012. Evaluation of benznidazole treatment combined with nifurtimox, posaconazole or AmBisome® in mice infected with *Trypanosoma cruzi* strains. Int. J. Antimicrob. Agents **40**:527–532. Doi: 10.1016/j.ijantimicag.2012.08.002
50. **Bustamante JM, Craft JM, Crowe BD, Ketchie SA, Tarleton RL.** 2014. New, combined, and reduced dosing treatment protocols cure *Trypanosoma cruzi* infection in mice. J. Infect. Dis. **209**:150−162. Doi: 10.1093/infdis/jit420.
51. **Hall BS, Wilkinson SR**. 2012. Activation of benznidazole by trypanosomal type I nitroreductases results in glyoxal formation. Antimicrob. Agents Chemother. **56**:115−123. Doi: 10.1128/AAC.05135-11

52. **Rajão MA, Furtado C, Alves CL, Passos-Silva DG, de Moura MB, Schamber-Reis BL, Kunrath-Lima M, Zuma AA, Vieira-da-Rocha JP, Borio Ferreira Garcia J, Mendes IC, Junho Pena SD, Macedo AM, Franco GR, de Souza-Pinto NC, de Medeiros MH, Cruz AK, Machado Motta MC, Ribeiro Teixeira SM, Machado CR.** 2014. Unveiling benznidazole's mechanism of action through overexpression of DNA repair proteins in *Trypanosoma cruzi*. Environ. Mol. Mutagen. **55**:309−321, Doi: 10.1002/em.21839.

List of figure captions.

Figure 1. Ruthenium complexes (**1-4**). (A) Representation of the complexes: *cis*-[RuCl(NO_2)(dppb)(5,5–mebipy)] (**1**); *cis*–[Ru(NO_2)$_2$(dppb)(5,5–mebipy)] (**2**); *ct*–[RuCl(NO)(dppb)(5,5–mebipy)](PF_6)$_2$ (**3**); *cc*-[RuCl(NO)(dppb)(5,5–mebipy)](PF_6) (**4**). N–N = 5,5'-dimethyl-2,2'–bipyridine (5,5'–mebipy) and P–P = 1,4-*bis*(diphenylphosphino)butane (dppb). (B) ORTEP-3 view of *cis*-[Ru(NO_2)$_2$(dppb)(5,5-mebipy)] (**2**) and the atom numbering scheme. Ellipsoids are drawn at the 30 % probability level.

Figure 2. Ruthenium complexes reduce the *in vitro* infection. Panel (A) shows the % of infection in comparison to untreated infected cells. Panel (B) shows the % of amastigotes / 100 macrophages in comparison to untreated. Panel (C) shows the parasite burden, calculated as % infected cells x mean number of amastigotes. Infected macrophages were treated for 6 h and then incubated for 4 days. Three independent experiments were performed. Error bars represent the standard error of the mean. *** p <0.0001 compared to untreated.

Figure 3. Ruthenium complex (**3**) increases NO in infected macrophages. Nitrite levels in infected macrophages determined 24 h after treatment. BALB/c peritoneal (panel A) and J774 (panel B) macrophages were infected with trypomastigotes and treated with 10 µM of complex (**3**) and (**5**). A positive control culture (+ ctr) was stimulated with IFN-γ and LPS. The negative control culture (-ctr) received no treatment or stimulus. Nitrite contents in the supernatant were estimated by the Griess nitrite test 24 h later. Values represent the mean±S.E.M. of three independent experiments. ***Compared to negative control (p <0.0001); ** compared to -ctr (p < 0.001).

Figure 4. Ruthenium complex (**3**) causes irreversible morphological impairments to the parasite. Scanning electron micrograph in panel (A) shows untreated trypomastigote and panel (B) shows treated parasite. Transmission electron micrographs in panels (C-F) are trypomastigotes and panels (G) and (H) are infected macrophages. Panel (C) are untreated trypomastigotes, panels (D-F) are treated parasites. Arrow in (D) indicates cytoplasmic vacuoles. Arrow in panel (E) indicates mitochondrial swelling. Arrow and asterisk in panel (F) indicate nuclear membrane disruption and myelin-like figures, respectively. Panel (G) shows untreated infected cells while panel (H) shows treated infected cells. Arrow in panel (H) indicates cytoplasmic vacuoles. Complex (**3**) was added at 2.1 µM and incubated for 24 h in trypomastigotes and 6 h in infected macrophages. GA = Golgi apparatus; K = kinetoplast, N = nucleus; M = mitochondria.

Figure 5. Ruthenium complex (**3**) induces parasite autophagy. Panel (A) shows untreated parasites, panel (B) shows treatment with 0.1 mg/mL rapamycin and panel (C) is treatment with 2.1 µM of ruthenium complex (**3**). Axenic trypomastigotes were incubated for 24 h and stained with MDC and infected macrophages were incubated for 6 h and then stained with anti-LC3B antibody and DAPI. Images were captured using a confocal microscope with a 60x oil-immersion objective at 3x zoom. DIC = differential interference contrast.

Figure 6. Ruthenium-based treatment causes parasite death by inducing necrosis. Trypomastigotes were treated with complex (**3**) for 36 h. Parasites were examined by flow cytometry with annexin V and PI staining. Cells plotted in each quadrant represent the following: lower left, double negative; upper left, PI single positive; lower right, annexin V single positive; upper right, PI and annexin V double positive. (A) Untreated; (B) Complex (**3**) at 2.5 µM; (C) Complex (**3**) at 5.0 µM; (D) Percentage of PI-positive cells. Values are means±S.D. of triplicate tests. (-ctr) = negative control. **Compared to negative control (ANOVA, p <0.05); *** compared to negative control (ANOVA, p < 0.0001).

Figure 7. Ruthenium complex (**3**) reduces acute infection and this is enhanced under drug combination with benznidazole. Parasitemia (panel A) and survival (panel B) of T. cruzi-infected mice (*n*=6/group) orally treated once-a-day for 5 consecutive days with 25 µmol/kg (26.6 mg/kg) or 75 µmol/kg (80 mg/kg) of complex (**3**). Bdz was given at 384 µmol/kg (100 mg/kg). Panel (A), sets (a), (b), (c), vehicle vs Bdz (p <0.001); vehicle vs (**3**) 25 µmol/kg (p <0.001); vehicle vs (**3**) 75 µmol/kg (p <0.001). In panel (B), log rank analysis, vehicle vs (**3**) 75 µmol/kg (p < 0.01); vehicle vs Bdz (p < 0.001). Bdz = benznidazole. The % of viable trypomastigotes (panel C) and of macrophages (panel D). Drug concentration is indicated in the x axis in µM and cell viability was recorded 24 h after incubation. Parasitemia (panel E) and survival (panel E) of infected mice (*n*=6/group) orally treated once-a-day with a drug combination of complex (**3**) and benznidazole. In panel (**E**), set (a) vehicle vs (**3**) (p <0.001); vehicle vs Bdz (p <0.01); vehicle vs drug combination (p <0.001); (b) vehicle vs (**3**) (p <0.05); vehicle vs drug combination (p <0.001); (c) vehicle vs (**3**) (p <0.05); vehicle vs Bdz (p <0.001); vehicle vs drug combination (p <0.001). In panel (F), log rank analyses revealed curves are not significantly different.

List of Figures and Tables

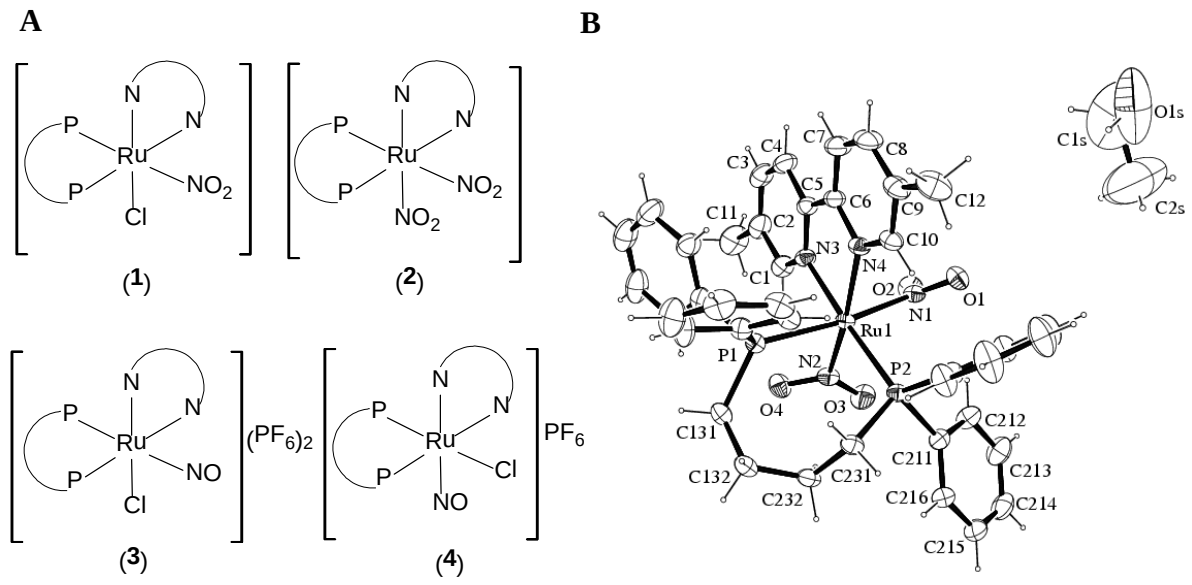

Figure 1.

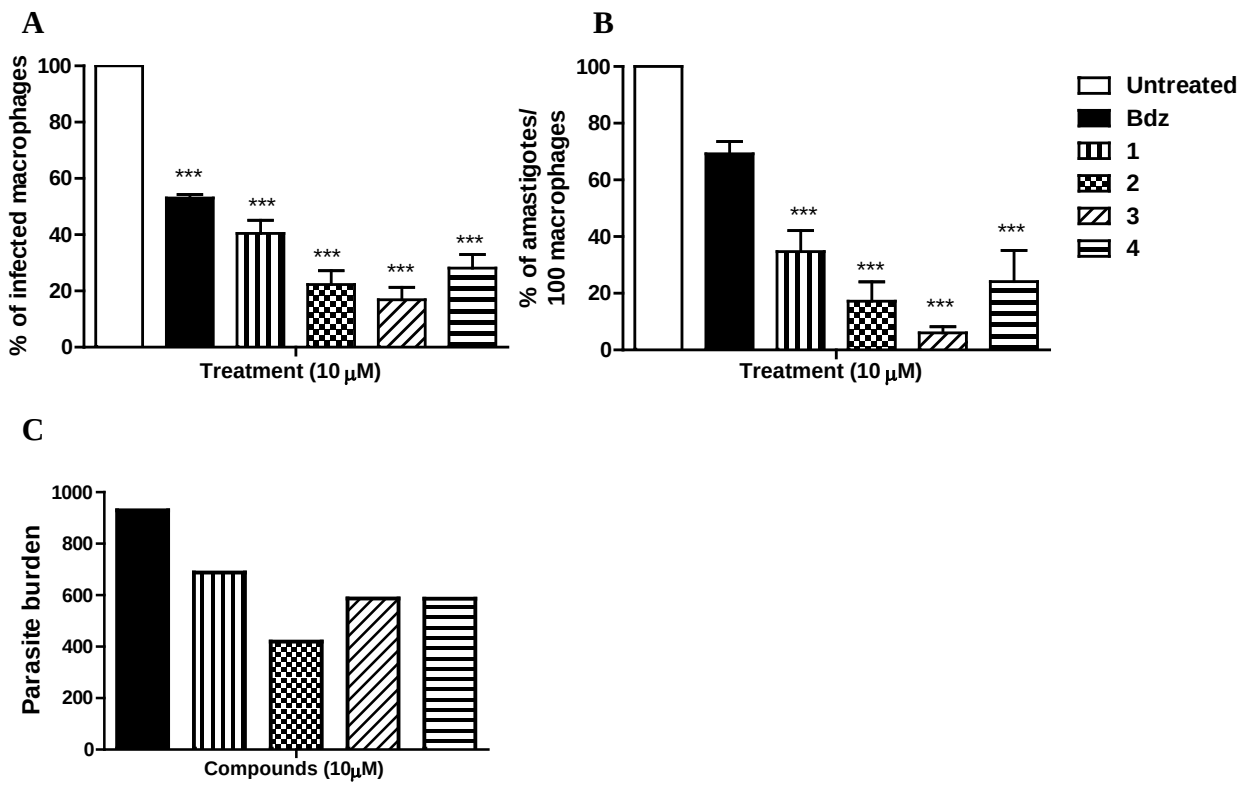

Figure 2.

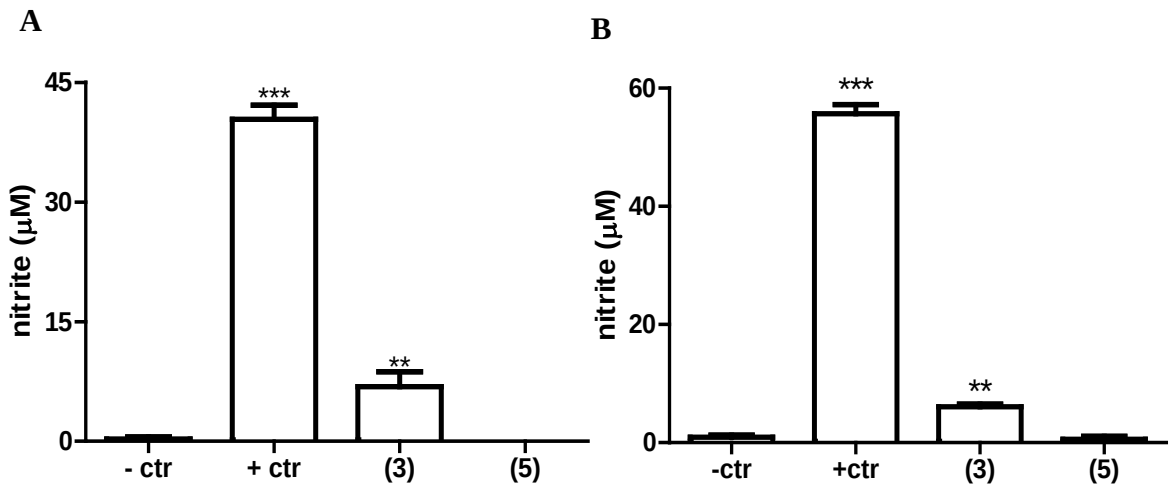

Figure 3.

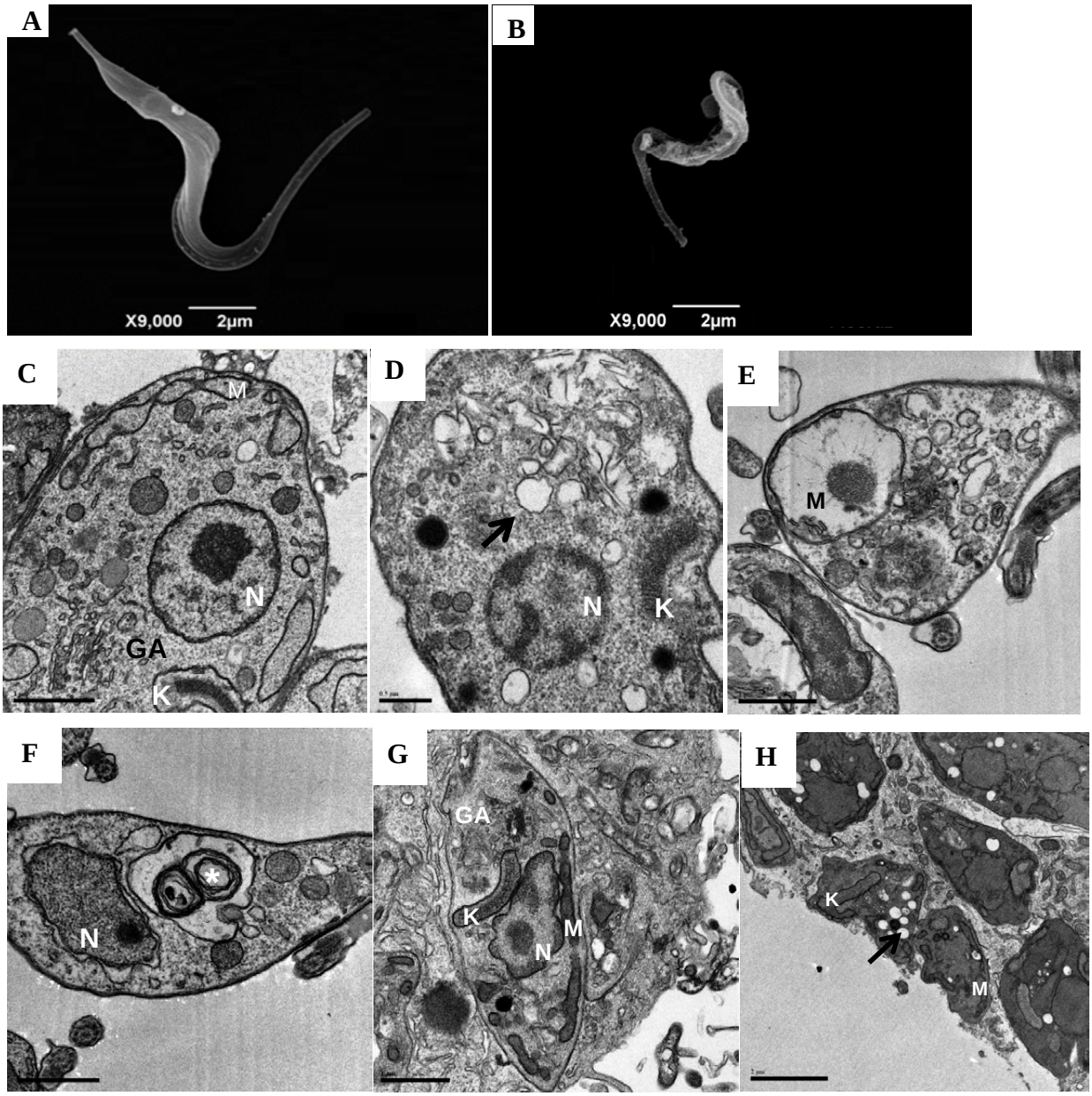

Figure 4.

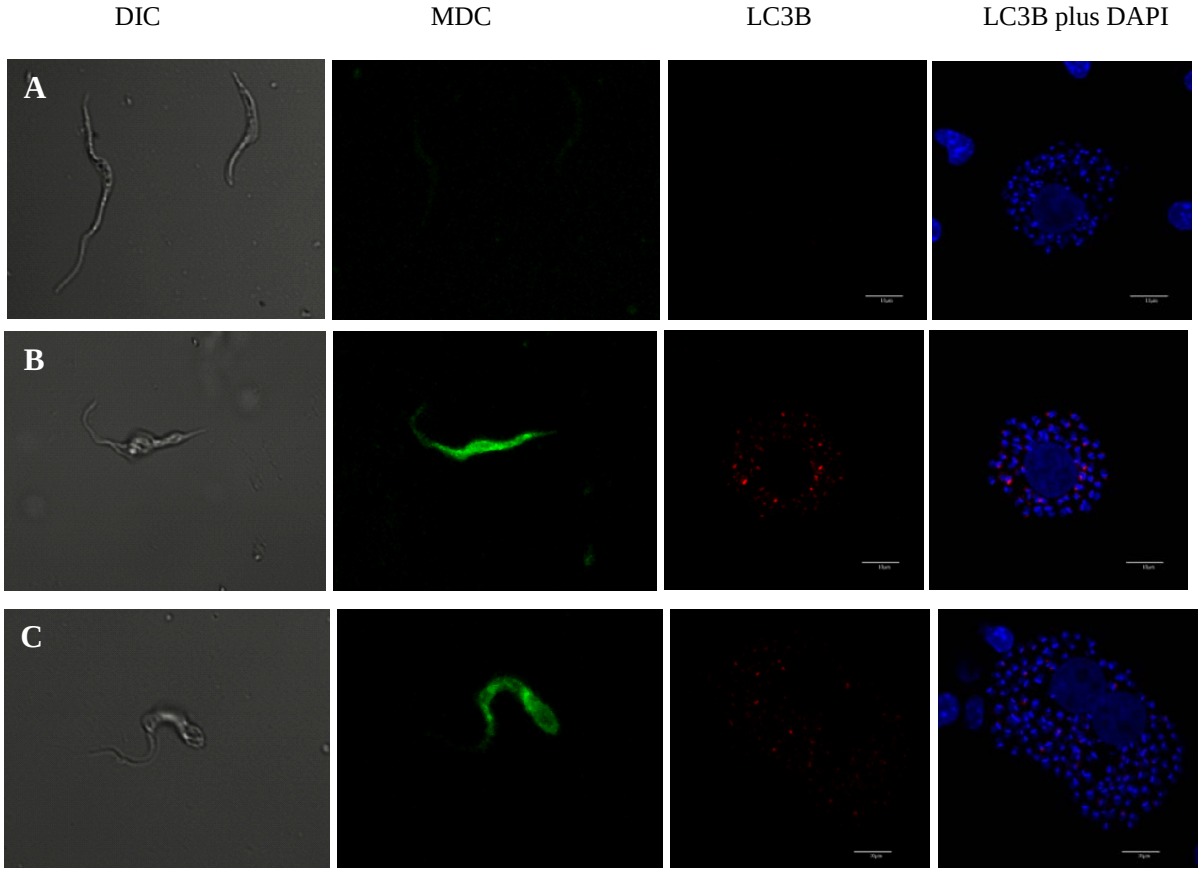

Figure 5.

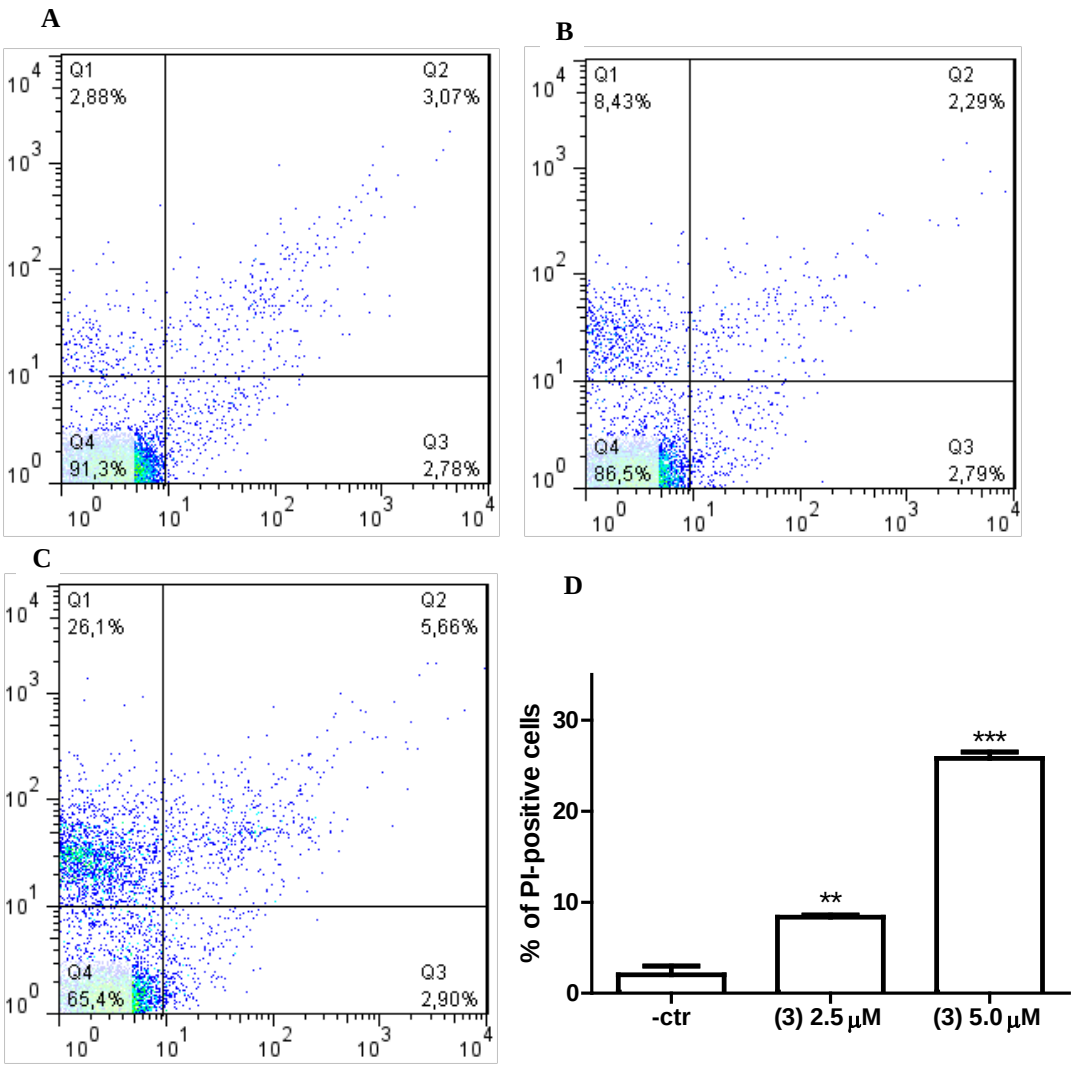

Figure 6.

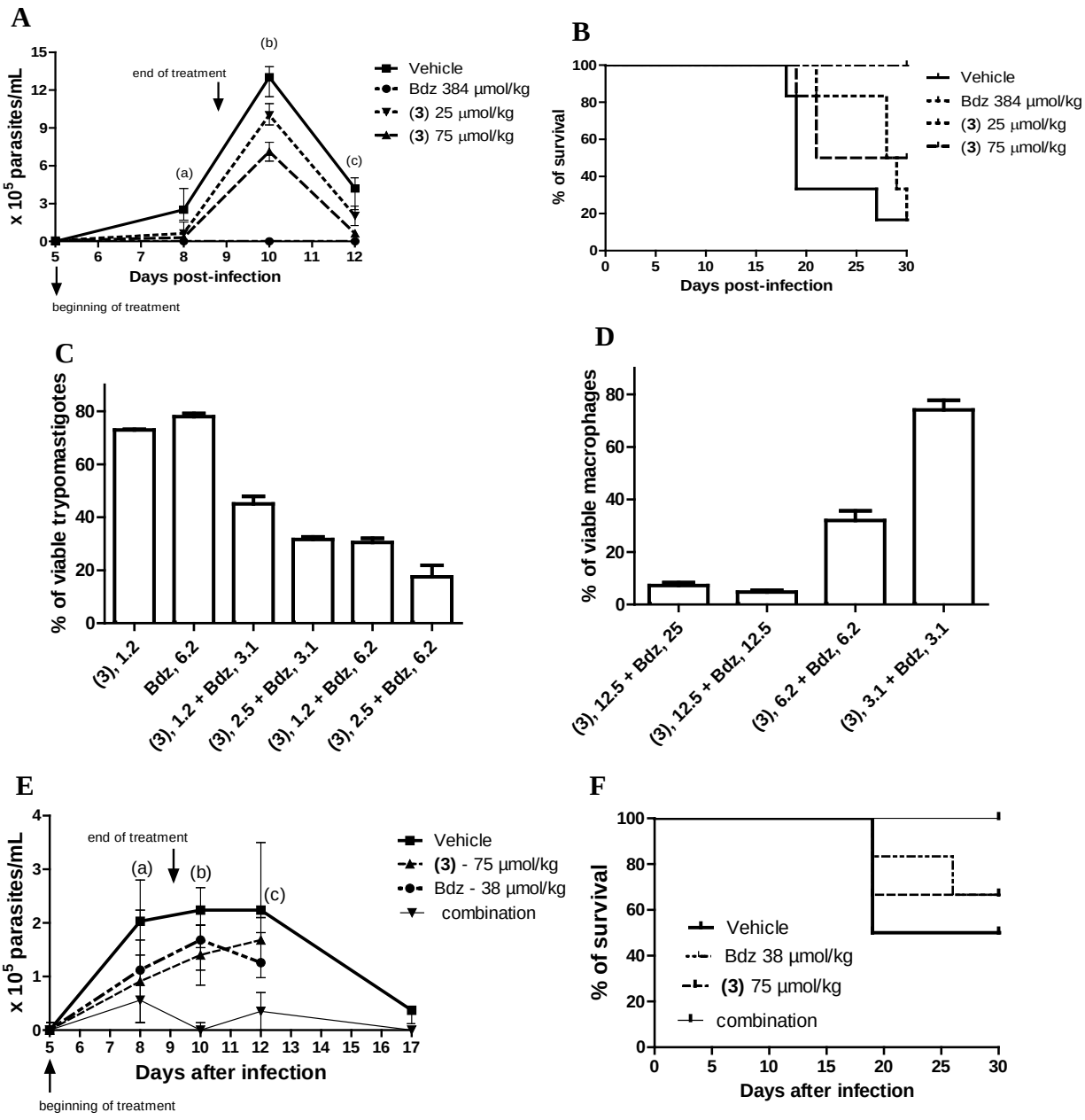

Figure 7.

Table 1: Crystal data and structure refinement of complex *cis*-[Ru(NO_2)$_2$(dppb)(5,5'-mebipy)] (**2**).

empirical formula	$[RuC_{42}H_{46}N_4O_5P_2]\cdot CH_3CH_2OH$
formula weight	849.84
temperature	293(2) K
wavelength	0.71073 Å
crystal system	triclinic
space group	*P*-1
unit cell dimensions	a = 10.2261(7) Å α = 74.904(2)° b = 12.2153(5) Å β = 74.660(3)° c = 17.4217(10) Å γ = 76.827(3)°
volume	1996.5(2) $Å^3$
Z	2
density (calculated)	1.414 Mg/m^3
absorption coefficient	0.522 mm^{-1}
F(000)	880
crystal size	0.30 x 0.26 x 0.10 mm^3
theta range for data collection	3.13 to 26.41°
index ranges	$-11 \le h \le 12$, $-15 \le k \le 15$, $-21 \le l \le 21$
reflections collected	15073
independent reflections	8129 [R(int) = 0.0217]
completeness to theta = 25.00°	99.0 %
absorption correction[32]	Gaussian
Max. and min. transmission	0.950 and 0.847
Refinement method	Full-matrix least-squares on F^2
computing[a]	COLLECT, HKL Denzo and Scalepack, SHELXL-97, SHELXS-97
data / restraints / parameters	8129 / 2 / 491
goodness-of-fit on F^2	1.056
final R index [I>2σ(I)]	R1 = 0.0378, wR2 = 0.1010
R index (all data)	R1 = 0.0442, wR2 = 0.1045
largest diff. peak and hole	0.611 and -0.640 $e.Å^{-3}$

[a] Data collection, data processing, structure solution and structure refinement respectively.

Table 2. Antiparasitic activity, host cell cytotoxicity and cruzain inhibition of ruthenium complexes (**1**–**5**).

Comp.	*T. cruzi*, Y strain		macrophages	cruzain
	epimastigotes IC_{50} ±S.E.M.(μM)[a]	trypomastigotes EC_{50} ±S.E.M.(μM)[b]	CC_{50}±S.E.M.(μM)[c]	IC_{50}±S.D.(μM)[d]
(**1**)	>100	8.4±1.1	> 100	30.2±7.3
(**2**)	16.6±0.6	2.9±0.2	50.5±0.1	>100
(**3**)	5.7±0.6	2.1±0.6	28.5±2.0	14.4±6.6
(**4**)	26.7±2.0	5.9±1.0	25.4±0.1	0.4±0.1
(**5**)	N.D.	> 100	> 100	59.8±4.6
Bdz	10.7±1.6	11.4±1.0	> 100	-
E64c	-	-	-	1.0±0.8nM

[a] Determined 5 days after incubation with complexes. [b] Determined 24 h after incubation with complexes. [c] Cell viability of BALB/c mouse macrophages determined 24 h after treatment. [d] Cruzain activity was determined 10 min after incubation. Values were calculated using concentrations in triplicate and two independent experiments were performed. IC_{50} = inhibitory concentration at 50 %. EC_{50} = effective concentration at 50 %. CC_{50} = cytotoxic concentration at 50 %. S.E.M. = standard error of the mean; S.D. = standard deviation. N.D. = not determined owing to lack of activity. Bdz = benznidazole. E64c = standard cruzain inhibitor.

Table 3. Antiparasitic activity in intracellular parasite, host cells cytotoxicity and selectivity index (SI) of ruthenium complexes (**1**–**5**).

Compounds	Amastigotes, IC_{50} ±S.E.M.(μM)[a]	Macrophages, CC_{50}±S.E.M.(μM)[b]	SI [c]
(**1**)	4.2±1.6	>100	>24
(**2**)	2.6±0.7	93.1±7.7	36
(**3**)	1.3±0.2	51.4±0.2	40
(**4**)	2.7±0.6	38.3±2.3	14
(**5**)	N.D.	> 100	N.D.
Bdz	14.0±0.3	>100	>7

[a] Cells were exposed to complexes for 6h and activity was determined 4 days after incubation with complexes. [b] Cell viability of BALB/c mouse macrophages determined 6 h after treatment. [c] SI is selectivity index, calculated by the ratio of CC_{50} (macrophages) and IC_{50} (amastigotes). IC_{50} and CC_{50} values were calculated using concentrations in triplicate and two independent experiments were performed. IC_{50} = inhibitory concentration at 50 %. CC_{50} = cytotoxic concentration at 50 %. S.E.M. = standard error of the mean; S.D. = standard deviation. N.D. = not determined owing to lack of activity. Bdz = benznidazole.

Table 4. Concentration reduction and combination indexes in trypomastigotes treated with ruthenium complex (**3**) and benznidazole.

Comp.	EC_{50} ±S.D.(μM)		CRI at EC_{50}	EC_{90} ±S.D.(μM)[a]		CRI at EC_{90}	CI at	
	alone	combination		alone	combination		EC_{50}	EC_{90}
Complex (**3**)	2.1±0.6	0.8±0.02	2.7±0.2	4.9±0.1	1.7±0.02	2.6±0.2	0.65±0.03	0.56±0.09
Bdz	11.4±1.0	4.1±0.1	3.5±0.1	25.8±0.8	8.7±0.1	4±0.8		

[a] EC_{50} and EC_{90} values were calculated using concentrations in duplicate and two independent experiments were performed. Cutoff: CI value of 0.3-0.7, synergism; 0.7-0.85, moderate synergism; 0.85-0.9, slight synergism; 0.9-1.1, additivity; > 1.1, antagonism. S.D = standard deviation; CRI. = Concentration reduction index. CI = Combination index. Bdz = benznidazole.